International Journal of
Molecular Sciences

MDPI

Article

Octafluoro-Substituted Phthalocyanines of Zinc, Cobalt, and Vanadyl: Single Crystal Structure, Spectral Study and Oriented Thin Films

Aleksandr Sukhikh, Darya Klyamer, Dmitry Bonegardt and Tamara Basova *

Nikolaev Institute of Inorganic Chemistry SB RAS, 3 Lavrentiev Pr., 630090 Novosibirsk, Russia
* Correspondence: tbasova@mail.ru

Abstract: In this work, octafluoro-substituted phthalocyanines of zinc, vanadyl, and cobalt ($MPcF_8$, M = Zn(II), Co(II), VO) were synthesized and studied. The structures of single crystals of the obtained phthalocyanines were determined. To visualize and compare intermolecular contacts in $MPcF_8$, an analysis of Hirshfeld surfaces (HS) was performed. $MPcF_8$ nanoscale thickness films were deposited by organic molecular beam deposition technique and their structure and orientation were studied using X-ray diffraction. Comparison of X-ray diffraction patterns of thin films with the calculated diffractograms showed that all three films consisted of a single crystal phase, which corresponded to a phase of single crystals. Only one strong diffraction peak corresponding to the plane (001) was observed on the diffraction pattern of each film, which indicated a strong preferred orientation with the vast majority of crystallites oriented with a (001) crystallographic plane parallel to the substrate surface. The effect of the central metals on the electronic absorption and vibrational spectra of the studied phthalocyanines as well as on the electrical conductivity of their films is also discussed.

Keywords: metal phthalocyanines; fluorine substituents; single crystal structure; thin films; X-ray diffraction; conductivity

Citation: Sukhikh, A.; Klyamer, D.; Bonegardt, D.; Basova, T. Octafluoro-Substituted Phthalocyanines of Zinc, Cobalt, And Vanadyl: Single Crystal Structure, Spectral Study and Oriented Thin Films. *Int. J. Mol. Sci.* **2023**, *24*, 2034. https://doi.org/10.3390/ijms24032034

Academic Editor: Elena Balashova and Boris B. Krichevtsov

Received: 29 December 2022
Revised: 16 January 2023
Accepted: 17 January 2023
Published: 19 January 2023

1. Introduction

Phthalocyanines (MPc) have been known for more than a hundred years but are still of wide interest to researchers not only as dyes and pigments but also as molecular semiconductors, catalysts, and photosensitizers. Due to the extensive π-system and the ability to form supramolecular ensembles in the form of columns of parallel packed molecules, they have a number of important and interesting properties. Today they are used in various branches of science and technology, such as chemistry [1,2], physics [3,4], and medicine [5–7].

An important advantage of phthalocyanines is the ability to vary their structure widely by replacing the central metal and substituents, both in the aromatic macrocycle and in axial positions. Such modification leads to a significant change in the solubility of phthalocyanine derivatives, as well as their optical, electrophysical, and catalytic properties [8–12]. For example, the introduction of fluorine substituents into the phthalocyanine ring leads to a decrease in their solubility in conventional organic solvents, but fluorinated phthalocyanines become capable of transferring into the gaseous phase without decomposition in a vacuum [13,14], which makes it possible to obtain their homogeneous thin films using a physical vapor deposition method. It has been shown that the introduction of fluorine substituents leads to a change in conductivity and transport properties [15]. For example, unlike ZnPc, which exhibits *p*-type semiconductor behavior, $ZnPcF_8$ and $ZnPcF_{16}$ are *n*-type semiconductors, while $ZnPcF_4$ can demonstrate am-

bipolar behavior. Due to these electrical properties, fluorinated metal phthalocyanines are widely used as active layers of diodes and organic field-effect transistors (OFET) [16–18]. Another important area of their application is the active layers of chemical sensors for the detection of hazardous gases and substances in aquatic environments [19–21]. To use phthalocyanines in electronic devices, it is important to obtain thin films with a controlled structure and ordering on various surfaces. The study of the structural features of their single crystals and the packing of molecules in thin films can reveal the influence of π–π interactions and other molecular contacts on the properties of phthalocyanine-based materials. It is also worth noting that the structure and phase composition of phthalocyanine films of nanoscale thickness may differ from the structure of their single crystals and powders [22–24]; for this reason, special attention should be paid to the study of the structural features of thin films since they determine the electrical and sensor properties.

Among fluoro-substituted metal phthalocyanines, hexadecafluoro-substituted derivatives are the most studied. The structure of single crystals of $MPcF_{16}$ (M=Cu, Co, Zn, Pd, Fe, Pb, VO) [22,25,26] and the structural features of their films [27,28] have already been reported in a number of publications. The effect of morphology and ordering in $MPcF_{16}$ films on their electrical properties and OFET characteristics has also been discussed by many researchers [29–31]. Recently we studied structures of single crystals and thin films of a series of tetrafluoro-substituted phthalocyanines bearing F-substituents both in the peripheral ($MPcF_4$-p, M=Co, Cu, Zn, Pd, Fe, Pb, VO) [13,32] and non-peripheral ($MPcF_4$-np, M= Co, Cu, Zn, Pd, Fe, Pb, VO) [23,33] positions in the phthalocyanine macroring. Similar to $MPcF_{16}$, $MPcF_4$ films are also widely studied as active layers of OFETs [34] and chemical sensors [33]. It has been shown that the introduction of different numbers of F-substituents leads to alteration of the intermolecular contacts and as a result a change in the crystal structure and packing of the phthalocyanine molecules. This also affects their thermodynamic [13] and electrical [35,36] properties as well as sensor performance [28]. At the same time, octafluoro-substituted metal phthalocyanines have not been studied in detail and work on the study of the structure of their single crystals and films have been sporadic. For example, Jiang et al. [37] refined the structures of $ZnPcF_8$ and $CuPcF_8$ single crystals and studied charge-carrier mobility in their single crystals. The structures of anionic salts of $CuPcF_8$ with tetrabutyl ammonium and (triphenylphosphoranylidene) ammonium were also investigated [38]. Brinkmann et al. [35] studied vapor-deposited $ZnPcF_8$ films using UV-vis absorption spectroscopy and scanning electron microscopy and investigated change in their current during exposure to oxygen. Several works have been devoted to the study of molecule–substrate interface states in ultrathin $ZnPcF_8$ films deposited onto single-crystal substrates using scanning tunneling microscopy and photoemission spectroscopy [39,40]. At the same time, crystals and films of other $MPcF_8$ derivatives have not yet been studied.

To fill this gap, octafluoro-substituted phthalocyanines of zinc, vanadyl, and cobalt ($MPcF_8$, M=Zn(II), Co(II), VO) were synthesized and studied in this work. The structures of single crystals of the obtained phthalocyanines were determined. To visualize and compare intermolecular contacts in $MPcF_8$, an analysis of Hirshfeld surfaces (HS) was performed. $MPcF_8$ nanoscale thickness films were deposited using the organic molecular beam deposition (OMBD) technique and their structure and orientation were studied using X-ray diffraction. The effect of the central metals on the electronic absorption and vibrational spectra of the studied phthalocyanines as well as on the electrical conductivity of their films is also discussed.

2. Results and Discussion

2.1. $MPcF_8$ Crystal Structures

Single crystals of $ZnPcF_8$, $CoPcF_8$, and $VOPcF_8$ were obtained as a result of sublimation in a vacuum (10^{-2} Torr). $ZnPcF_8$ crystals form as relatively large clusters up to 1 mm

in length and 60 μm in width. $CoPcF_8$ crystals grow in the form of thin needles or long ribbons (up to 300 μm long, 30 microns wide, and less than 10 microns thick), with a tendency to bend and split into several smaller crystals. $VOPcF_8$ crystals have the form of small (<100 μm wide and <30 μm thick) elongated hexagonal plates. All crystals have a dark purple color and a metallic luster typical of phthalocyanines. Unit cell parameters and refinement statistics for $MPcF_8$ are given in Table 1. The main intermolecular and interatomic distances in $MPcF_8$ are summarized in Table 2.

Table 1. Unit cell parameters and refinement statistics for $MPcF_8$.

Compound	**$ZnPcF_8$**	**$CoPcF_8$**	**$VOPcF_8$**
Empirical formula	$C_{32}H_8F_8N_8Zn$	$C_{32}H_8F_8N_8Co$	$C_{32}H_8F_8N_8OV$
Formula weight	721.83	715.39	723.40
Temperature/K	150	150	150
Crystal system	triclinic	triclinic	triclini
Space group	P−1	P−1	P−1
a/Å	8.2156(5)	3.6061(2)	9.0821(5)
b/Å	11.5255(7)	13.0280(7)	10.3447(5)
c/Å	14.0379(8)	13.4901(7)	13.9293(8)
α/°	78.693(2)	84.097(2)	98.578(2)
β/°	73.840(2)	89.055(2)	92.165(2)
γ/°	89.047(2)	82.976(2)	92.909(2)
Volume/Å^3	1250.92(13)	625.67(6)	1291.01(12)
Z	2	1	2
ϱ_{calc}g/cm^3	1.916	1.899	1.861
μ/mm^{-1}	1.087	0.791	0.492
Radiation	MoKα (λ = 0.71073)	MoKα (λ = 0.71073)	MoKα (λ = 0.71073)
2Θ range for data collection/°	3.082 to 61.038	3.036 to 51.362	4.594 to 56.68
Reflections collected	15,790	9899	20,656
Independent reflections	7629 [R_{int} = 0.0271, R_{sigma} = 0.0399]	2377 [R_{int} = 0.0489, R_{sigma} = 0.0476]	6423 [R_{int} = 0.0375, R_{sigma} = 0.0443]
Data/restraints/parameters	7629/0/442	2377/0/223	6423/0/451
Goodness-of-fit on F^2	1.030	1.063	1.039
Final R indexes [I > = 2σ (I)]	R_1 = 0.0354, wR_2 = 0.0886	R_1 = 0.0539, wR_2 = 0.1314	R_1 = 0.0518, wR_2 = 0.1393
Final R indexes [all data]	R_1 = 0.0551, wR_2 = 0.0978	R_1 = 0.0760, wR_2 = 0.1427	R_1 = 0.0762, wR_2 = 0.1552
Largest diff. peak/hole/e Å^{-3}	0.50/−0.35	1.05/−0.36	1.22/−0.39
Number in CCDC	2177575	2177576	2177577

Table 2. Intermolecular and interatomic distances in $MPcF_8$.

Distances	**$ZnPcF_8$**	**$CoPcF_8$**	**$VOPcF_8$**
between layers, Å	3.173	N/A	3.382
between molecules, Å	3.217	3.299	3.411/3.354
d_{norm} (min/max), Å	−0.1495/1.3175	−0.1985/1.3833	−0.1477/1.4484
metal…metal, Å	4.867	3.606	5.871
C…C/C…N close contacts, Å	3.211−3.260 < 3.235>	3.271−3.275 < 3.273>	3.204−3.352 < 3.288>
O…H close contacts, Å	N/A	N/A	2.409−2.505 < 2.457>
F…H close contacts, Å	2.354−2.401 < 2.368>	2.440	2.404−2.509 < 2.451>
F…F close contacts, Å	N/A	N/A	2.864
π…π interactions (angle/distance/shift)	2.603°/3.232 Å/0.777 Å 1.219°/3.230 Å/0.786 Å	0°/3.251−3.357 Å/1.318−1.561 Å	4.454°/3.424 Å/1.123 Å 3.995°/3.228 Å/1.068 Å

Figure 1 shows the molecular packing for $ZnPcF_8$. $ZnPcF_8$ crystallizes in a triclinic system with Z=2, which is identical to the $ZnPcF_8$ crystal structure previously reported by Jiang et al. [37]. $ZnPcF_8$ molecules are arranged in layers along the *c* axis (Figure 1a). This is typical for planar phthalocyanines, which usually crystallize in uniform stacks or in a

"herringbone" pattern. The distance between layers is 3.173 Å and between the planes of adjacent molecules is 3.217 Å; the angle between the layer and the individual molecule (planes constructed through all atoms except hydrogen) is only 0.66°. When viewed along the *a* axis (Figure 1b), it seems that $ZnPcF_8$ molecules form stacks, but the molecules inside the stack are staggered, so that the central metals do not lie on the same line as in other planar phthalocyanines (Figure 1c) [13].

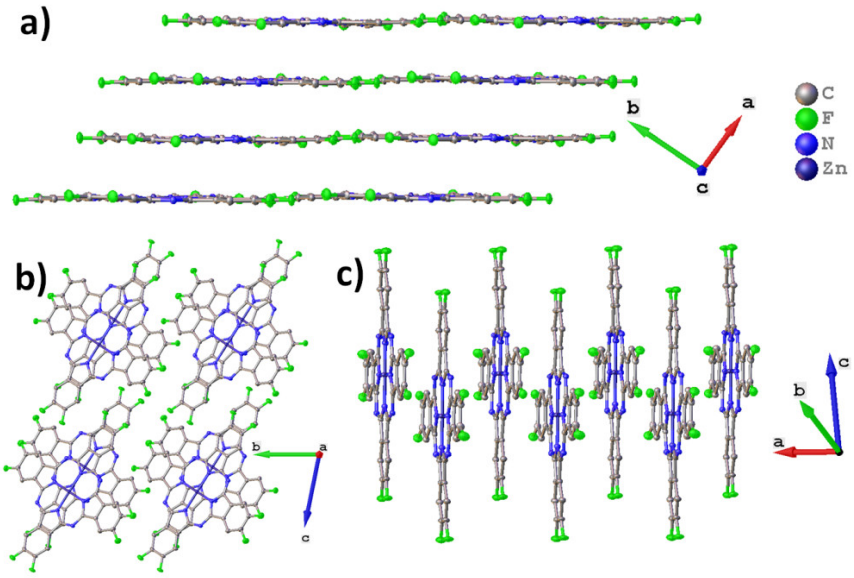

Figure 1. Molecular packing diagrams for $ZnPcF_8$: molecular layers along the *c* axis (**a**), stacks along the *a* axis (**b**), and arrangement of molecules in an individual stack (**c**).

Molecular packing diagrams for $CoPcF_8$ are shown in Figure 2. $CoPcF_8$ crystallizes in a triclinic system with Z=1 and is isostructural to the previously studied $CuPcF_8$ [15,37], as well as peripherally substituted tetrafluorinated cobalt phthalocyanine ($CoPcF_4$-p) [13] and unsubstituted α-CoPc [41].

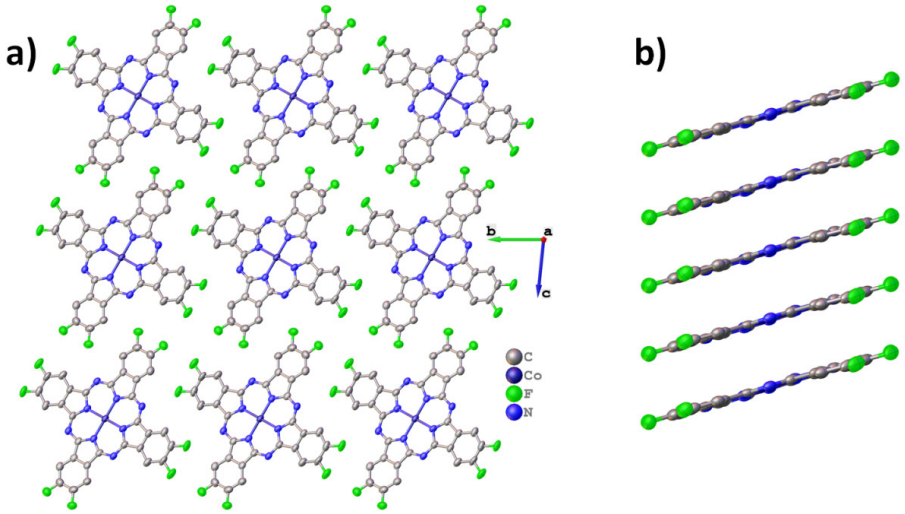

Figure 2. Molecular packing diagrams for $CoPcF_8$: molecular stacks along the *a* axis (**a**), molecular arrangement inside the individual stack (**b**).

$CoPcF_8$ molecules are packed in uniform stacks along the *a* axis (Figure 2a) with a distance of 3.299 Å between adjacent molecules inside the stack and a stacking angle of 23.81° (the angle between the normal to the molecule plane and the stacking axis). For

comparison, these values are 3.318Å and 24.70° in $CoPcF_4$-p and 3.414 Å and 24.58° in α-CoPc. The molecular arrangement inside the individual stack is shown in Figure 2b.

Unlike zinc and cobalt phthalocyanines, vanadyl phthalocyanine molecules are not planar, resulting in a different packing style. For instance, the triclinic polymorph of VOPc and $VOPcF_4$-p form molecular chains, in which one "facing up" molecule is adjacent to two "facing down" molecules. At the same time, $VOPcF_{16}$ and $VOPcF_4$-np form molecular layers, where one "facing up" molecule is adjacent to four "facing down" molecules [13,23,42]. Molecular packing diagrams for $VOPcF_8$ are shown in Figure 3. As can be seen when viewed along the *b* axis, $VOPcF_8$ molecules do not form continuous 2D layers, since the only type of interaction between molecules along the *c* axis is close F...F and F...H contacts (Figure 3a). Instead, $VOPcF_8$ molecules are arranged along the *a* axis with alternating "up" and "down" configurations (Figure 3b,c). The gaps between the molecules in the chain are filled with two oxygen atoms belonging to molecules from two neighboring chains; the distance between these oxygen atoms is 3.300 Å. This molecular arrangement differs significantly from other fluorinated vanadyl phthalocyanines, where the gap between two molecules (chain packing) or four molecules (layered packing) is occupied by only one oxygen atom.

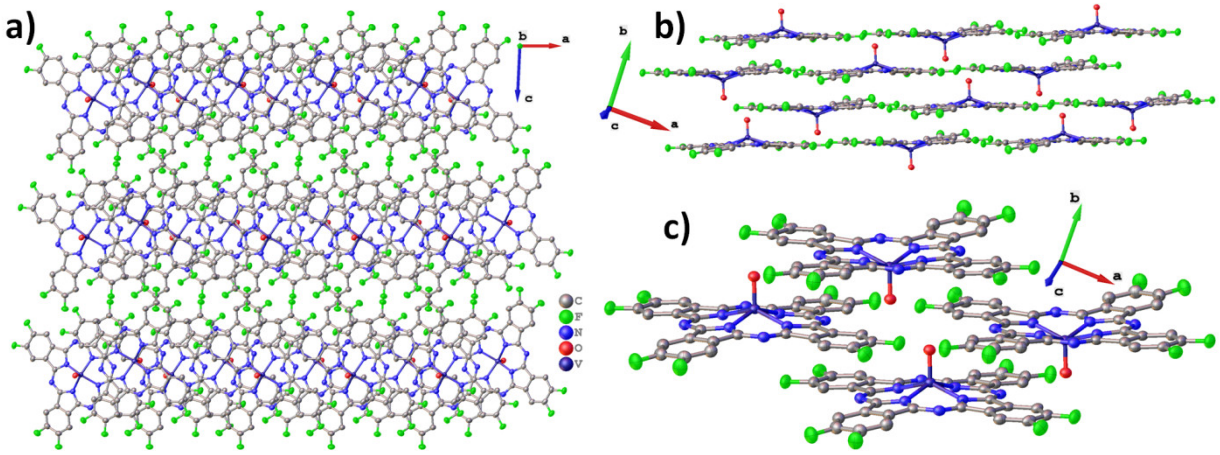

Figure 3. Molecular packing diagrams for $VOPcF_8$: the packing motif along the *a* axis (**a**), the arrangement of molecules inside an individual layer (**b**), and a close-up view of the arrangement of neighboring molecules inside the layer (**c**).

2.2. Hirshfeld Surface Analysis

To better analyze and visualize intermolecular interactions in $MPcF_8$, Hirshfeld surfaces (HS) generated in CrystalExplorer 21.5 [43] and mapped with d_{norm} (normalized contact distance) and shape index properties, were used. Figure 4 shows HS for $MPcF_8$ molecules mapped with the d_{norm} property. By default, CrystalExplorer selects an individual d_{norm} scale range for each Hirshfeld surface based on the minimum/maximum values for the specified surface. These values are −0.1495/1.3175 for $ZnPcF_8$, −0.1985/1.3833 for $CoPcF_8$, and -0.1477/1.4484 for $VOPcF_8$, which means that the crystal structure of $CoPcF_8$ contains stronger close contacts compared to others. Thus, an arbitrary range of −0.2–1.45 was chosen for the convenience of visual comparison between all three $MPcF_8$ compounds. The front and back sides of the HS of $ZnPcF_8$ have four red spots arranged in a square shape, which correspond to $C_\alpha \ldots C_\delta$ close contacts between neighboring molecules in the range of 3.211 Å–3.260 Å (mean value 3.235 Å). Close H…F and F…H contacts with the shortest distance of 2.354 Å are also well visualized at the edges of the molecules (Figure 4a).

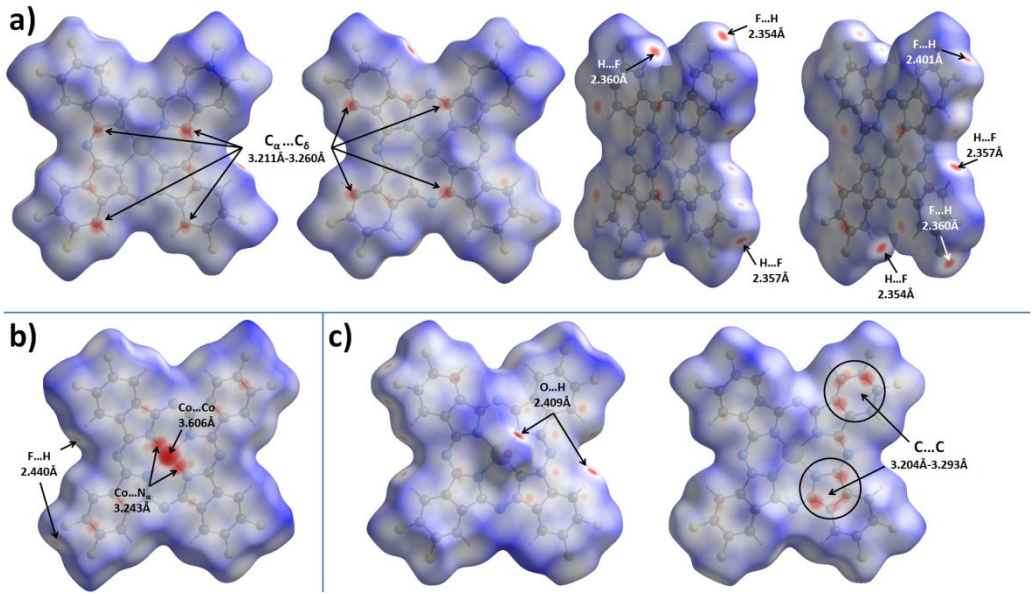

Figure 4. Hirshfeld surfaces for $ZnPcF_8$ (**a**), $CoPcF_8$ (**b**), and $VOPcF_8$ (**c**), mapped with the d_{norm} property in the range of −0.2–1.45.

Figure 4b shows only one side of $CoPcF_8$ HS, since the crystal structure of $CoPcF_8$ contains a single centrosymmetric molecule, which means that the front and back sides of $CoPcF_8$ HS are identical. It contains several red spots, which correspond to various close contacts between carbon atoms of neighboring molecules in the stack. These short contacts are much less noticeable than in the case of $ZnPcF_8$ since $CoPcF_8$ molecules are located 0.087 Å further apart than in $ZnPcF_8$. Instead, $CoPcF_8$ HS is dominated by three large red spots in the center, which correspond to Co…Co close contact with a distance of 3.606 Å and two reciprocal Co…N_α close contacts (3.243 Å). The presence of these close contacts is due to the tendency of the cobalt cation to have octahedral coordination. The angle between the close Co...N_α contact and the normal to the square formed by the four N_α atoms of the $CoPcF_8$ molecule is 174.31°, which is close to 180° for an ideal octahedron. The distance of Co-N_α in the molecule is 1.915 Å, while the distance between Co and N_α of the adjacent molecule in the stack is 3.243 Å. The side of $CoPcF_8$ HS is characterized by four weak red dots, which correspond to four close F...H contacts of 2.440 Å. Although $CoPcF_8$ is isostructural with $CoPcF_4$-p [13], the contacts between the molecules in their adjacent stacks are different. There are four red spots that correspond to close contacts F...H on HS of both $CoPcF_4$-p and $CoPcF_8$, but these contacts in $CoPcF_4$-p are shorter by 0.139 Å than in the case of $CoPcF_8$.

There are two prominent red spots, which correspond to a reciprocal pair of close O…H contacts (2.409 Å), and several dull red spots, which correspond to various C…C contacts and one H…F contact (2.404 Å) on the front side of $VOPcF_8$ HS (Figure 4c). Similar O…H close contacts were also observed in the case of the triclinic-II polymorph of VOPc (2.431 Å) [42] and $VOPcF_4$-p (2.441 Å) [13]. The back side of $VOPcF_8$ HS contains two clusters of red dots, which correspond to close contacts between carbon atoms in the pyrrole fragment of one molecule and carbon atoms in the benzene fragment of a neighboring one (3.204–3.293 Å, mean value 3.254 Å). Despite the large number of F-substituents, the F…H and F…F interactions are less pronounced than in $VOPcF_4$-p [13], which is characterized by very strong F…F interactions with the closest distance between fluorine atoms of only 2.281 Å.

Figure 5 shows HS mapped with the shape index property, which is very sensitive to small changes in surface curvature, especially for flat areas with a small overall curvature. In particular, this allows for identifying weak π–π interactions between phthalocyanine molecules, which are displayed on HS in the form of pairs of blue and red trian-

gles arranged in the form of an hourglass. Neighboring molecules are drawn on top of HS for better visualization of π–π interactions.

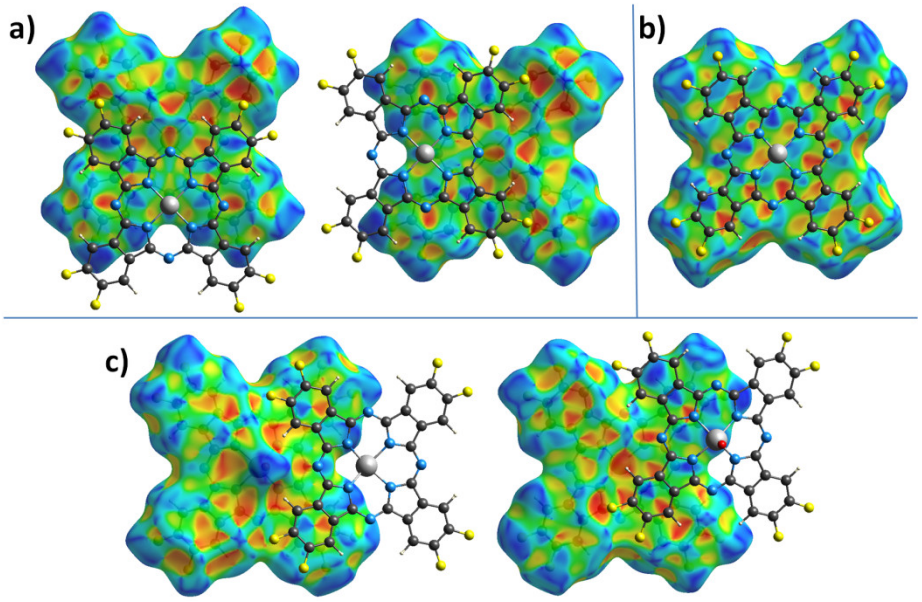

Figure 5. Hirshfeld surfaces for $ZnPcF_8$ (**a**), $CoPcF_8$ (**b**), and $VOPcF_8$ (**c**) molecules, mapped with the shape index property.

The front side of $ZnPcF_8$ HS shows π–π interactions between two pairs of pyrrole moieties. The back side also has these interactions, but it is rotated by 90° relative to the front surface. This means that among four pyrrole moieties in each $ZnPcF_8$ molecule, one fragment participates in two π–π interactions, two pyrrole fragments are involved in one π–π interaction each, and the last pyrrole fragment does not participate in any π–π interactions. The angle/distance/shift values for the π–π interactions between pyrrole fragments in $ZnPcF_8$ are 2.603°/3.232 Å/0.777 Å and 1.219°/3.230 Å/0.786 Å.

$CoPcF_8$ HS mapped with the shape index property has pairs of red and blue triangles in each benzene and pyrrole moiety, as well as in each of the four segments of the central macrocycle, which means that the whole $CoPcF_8$ molecule is involved in π–π interaction with neighboring molecules in the stack. The same character of interactions is also observed in α-CoPc [41] and $CoPcF_4$-p [13]. The angle values for π–π interactions are 0° for each fragment, while distance and shift are in the range of 3.251–3.357 Å and 1.318–1.561 Å, respectively.

The front side of the $VOPcF_8$ HS shows the π–π interaction between benzene moieties of neighboring molecules with the angle/distance/shift values of 4.454°/3.424 Å/1.123 Å, while the back surface is characterized by π–π interactions between a benzene moiety of one molecule and a pyrrole fragment of another molecule with angle/distance/shift values of 3.995°/3.228 Å/1.068 Å.

Thus, the introduction of eight F-substituents has different effects on the phthalocyanines of various metals. In the case of $CoPcF_8$, this effect is negligible and $CoPcF_8$ remains isostructural with its tetrafluoro-substituted analogue $CoPcF_4$-p [13]. However, in the case of $ZnPcF_8$, this leads to a complete change in the packing motif from conventional stacks to 2D molecular layers formed by staggered molecular stacks, which reduces the number of π–π interactions between neighboring molecules compared to $ZnPcF_4$-p [44]. $VOPcF_8$ molecules are packed into interconnected molecular chains, which can be considered as a cross between the molecular chains in the triclinic polymorph of VOPc-II and 2D molecular layers in $VOPcF_{16}$. Although the nature of the π–π interactions between neighboring molecules of $VOPcF_8$ does not differ much from other fluorinated vanadyl phthalocyanines, the same cannot be said about close F...F and F...H contacts.

Compared to $VOPcF_4$-p, F...F close contacts in $VOPcF_8$ are much less noticeable, which may lead to better crystallinity and lower micro stresses in the crystal lattice.

2.3. Vibrational Spectra of $MPcF_8$

IR and Raman spectra of $MPcF_8$ powders are shown in Figure 6a,b. The bands in the range from 1350 to 1620 cm^{-1}, which are assigned mostly to C=C and C=N stretching vibrations, are similar to those of tetrafluoro-substituted derivatives [45], while there is a noticeable difference in the position and intensities of bands with a significant contribution of C-F, C_β-C_γ-F, and C_β-C_γ-H vibrations in the range from 900 to 1350 cm^{-1}.

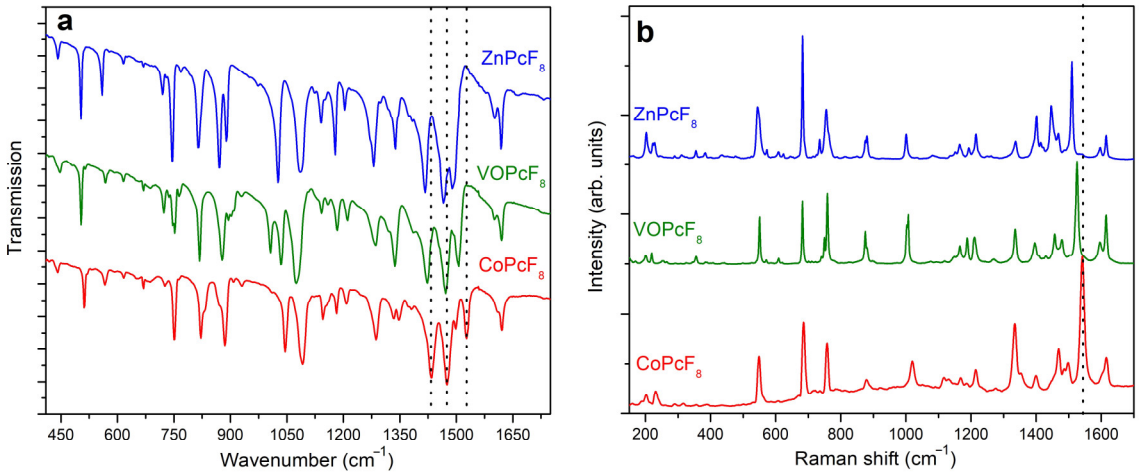

Figure 6. IR (**a**) and Raman (**b**) spectra of $MPcF_8$ (M=Co, VO, Zn).

The introduction of more F-substituents into the phthalocyanine macrocycle leads also to alterations in the range of 600–900 cm^{-1} in both IR and Raman spectra in comparison with $MPcF_4$ derivatives. The bands in this region corresponding mostly to M-N_α stretching vibrations and macroring deformations are mixed with C-C-H deformations and C-F stretching [45]. An increase in the number of withdrawing F-substituents and, as a consequence, a decrease in the number of C-C-H fragments leads to a change in the intensity and the form of vibrations in this region.

It is known that the range from 1350 to 1550 cm^{-1} in the vibrational spectra of metal phthalocyanines is considered as a "marker" of central metals. Similar to unsubstituted, tetrafluorinated, and perfluorinated MPc [45–48], $MPcF_8$ exhibits bands dependent on central metals in this spectral region. For example, the band at 1528 cm^{-1} in the IR spectrum of $CoPcF_8$ shifts to 1506 and 1492 cm^{-1} when passing to $VOPcF_8$ and $ZnPcF_8$, respectively (Figure 6a). The bands at 1434 cm^{-1} in the IR spectrum of $CoPcF_8$ are also observed at lower wavenumbers in the spectra of $VOPcF_8$ and $ZnPcF_8$. In the Raman spectra, the band, which is most sensitive to the central metal, lies at 1542 cm^{-1} for $CoPcF_8$ and shifts to 1526 cm^{-1} and 1510 cm^{-1} in the spectra of $VOPcF_8$ and $ZnPcF_8$, respectively (Figure 6b). According to the DFT calculations carried out in previous works [45–48], these bands are assigned to the displacements of C_α-N_β-C_α bridges between isoindole groups in the MPc macrocycle and the change of the cavity size during the macrocycle vibration. For this reason, the shift of these bands is in good correlation with the cavity size (more precisely, with the N_α-M-N_α distance) in the phthalocyanine molecules. Indeed, similarly to other phthalocyanine derivatives, the experimental N_α-M-N_α distance in $MPcF_8$ increases in the order of Co (3.83 Å) > VO (3.91 Å) > Zn (3.97 Å).

2.4. Study of $MPcF_8$ Powders and Thin Films by XRD and UV-vis Spectroscopy

XRD patterns for bulk powders and as-deposited thin films of $MPcF_8$ are shown in Figure 7. The XRD patterns of the films heated at 200 °C for 3 h in air are also given because it is known that films of some metal phthalocyanines undergo a phase transition when heated [49,50].

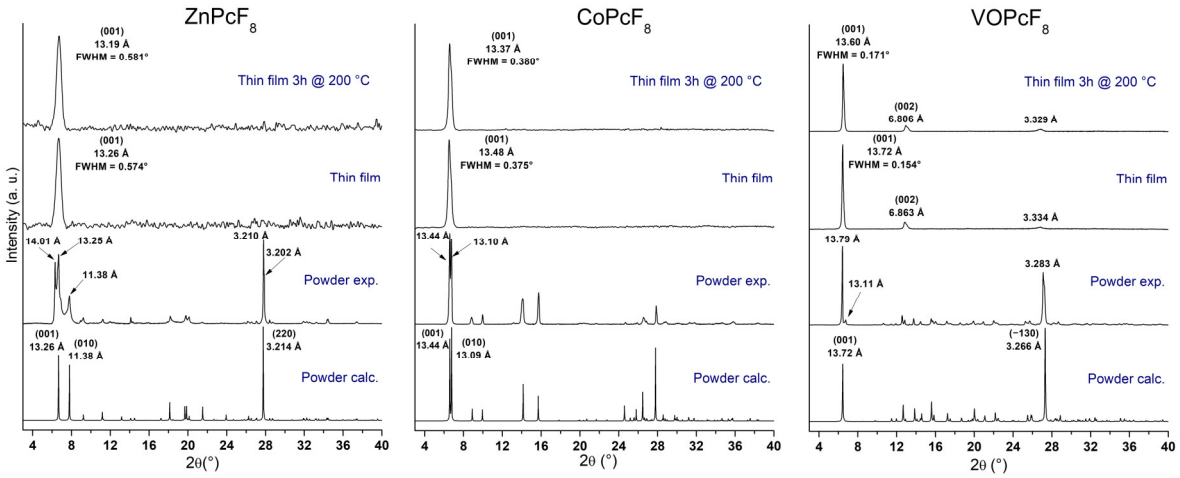

Figure 7. XRD patterns for $MPcF_8$ powders (experimental and calculated) and thin films before and after heating for 3 h at 200 °C.

Polycrystalline $MPcF_8$ powders were obtained by gradient sublimation in a vacuum. Among the three investigated phthalocyanines, only the $CoPcF_8$ powder pattern completely coincides with the calculated one. Two small diffraction peaks with d = 13.11 Å and d = 8.317 Å on the XRD pattern of $VOPcF_8$ powder do not coincide with the calculated powder pattern and belong to another crystalline phase of $VOPcF_8$, which is present in an insignificant amount in the investigated powder.

$ZnPcF_8$ powder contains two crystal phases mixed in a comparable amount. The structural data of the first phase are presented in Table 1. We also tried to isolate single crystals of the second phase of $ZnPcF_8$ but only one small (less than 30 μm in length and 5 μm in thickness) defective needle crystal, which did not show any diffraction spots with a resolution better than 3 Å on the detector frame with a collection time of 300 s/frame, was found. For this reason, only its unit cell parameters (measured by ~100 collected reflections) were determined: a = 3.655(7) Å; b = 13.38(2) Å; c = 13.67(2) Å; α = 85.21(4)°; β = 88.52(9)°; γ = 82.36(6)°; and V = 660(3) Å^3. According to the unit cell parameters, the second phase of $ZnPcF_8$ is isostructural with $CoPcF_8$ and $CuPcF_8$.

A comparison of XRD patterns of thin films with the calculated diffractograms shows that all three films consist of a single crystal phase, which corresponds to the crystal structure data. Only one strong diffraction peak corresponding to the plane (001) is observed on the diffraction pattern of each film, which indicates a strong preferred orientation with the vast majority of crystallites oriented with a (001) crystallographic plane parallel to the substrate surface. Two additional weak diffraction peaks are observed on the diffractogram of the $VOPcF_8$ film; the peak with d = 6.863 Å corresponds to the plane (002), while the peak at 3.334 Å does not exactly coincide with the plane (004), which has d = 3.432 Å. This may be due to the fact that the preferred orientation of the $VOPcF_8$ film is not ideal, and the peak at 3.334 Å is actually a mixture of (004) and (−130) peaks, which are noticeable in the powder diffraction pattern.

Since all $MPcF_8$ thin films have strong a preferred orientation with a known plane of preferred orientation, it is possible to calculate the angle between molecules and the substrate surface using the data on the structure of single crystals. The angle values are 70.36° for $ZnPcF_8$, 77.17° for $CoPcF_8$, and 86.82° for $VOPcF_8$. The scheme of the orientation of $MPcF_8$ molecules in the thin films relative to the substrate surface is shown in Figure 8.

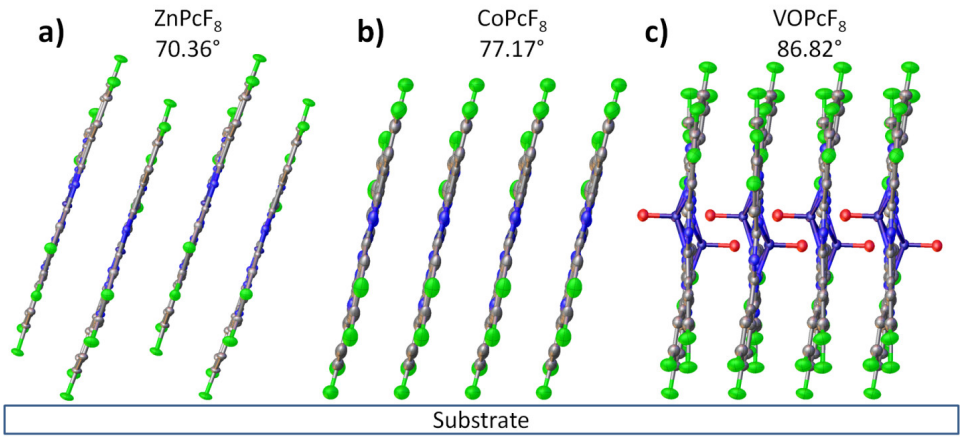

Figure 8. Orientation of $ZnPcF_8$ (**a**), $CoPcF_8$ (**b**), and $VOPcF_8$ (**c**) molecules in the thin films relative to the substrate surface.

UV-vis spectra of the films are given in Figure 9 in comparison with the spectra of $MPcF_8$ solutions in THF. All spectra contain a typical Q-band, which is attributed to the electron transitions from HOMO a_{1u} to the LUMO e_g and is very sensitive to the surrounding of an MPc molecule and intermolecular interactions [51,52].

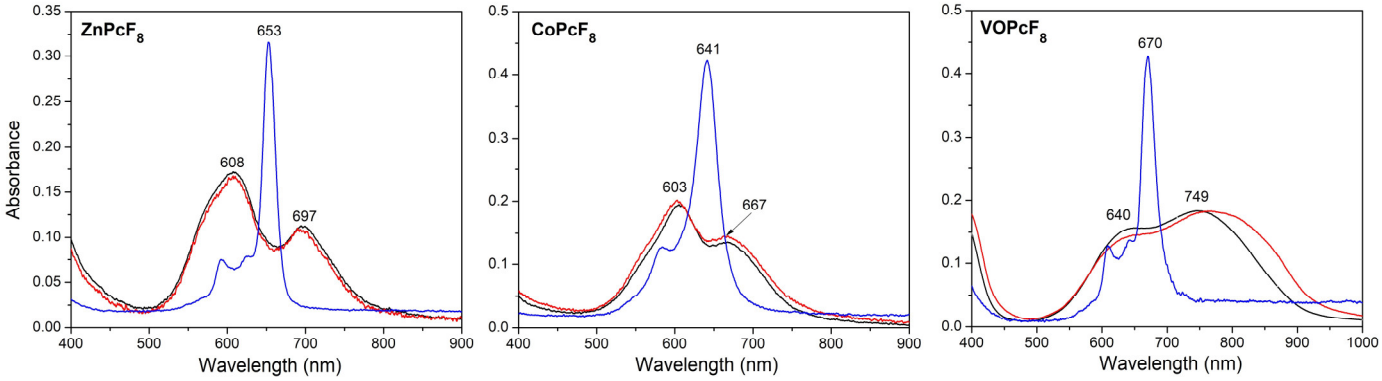

Figure 9. Optical absorption spectra of $MPcF_8$ (M=Zn, Co, VO) solutions in THF (blue lines) and films deposited on glass slides before (black lines) and after heating at 200 °C for 3 h (red lines).

The maxima of the Q-bands in the UV-vis spectra of $CoPcF_8$ and $ZnPcF_8$ solutions are located at 641 and 653 nm, respectively. The Q-band in the spectrum of a $CoPcF_8$ film deposited on a glass slide is split into two components Q_I and Q_{II} with maxima at 603 and 667 nm. This spectrum is similar to those for $CoPcF_4$ [53] and α-CoPc [54]. The Q-band splitting is due to intermolecular interaction and different arrangements of molecules relative to each other in a unit cell. According to the XRD data, $CoPcF_8$ is isostructural with them. The UV-vis spectrum of $ZnPcF_8$ also contains two Q-band components; however, the difference between their wavelengths is noticeably larger: Q_I at 608 nm and Q_{II} at 697 nm. The packing of molecules in $ZnPcF_8$ differs from that in $CoPcF_8$. As it was shown above, the $ZnPcF_8$ molecules are staggered inside the stack. The UV-vis spectrum of a $VOPcF_8$ film exhibits a broad red-shifted Q-band, which is similar to that in the spectra of non-planar VOPc and TiOPc derivatives [55] as well as $VOPcF_4$ [23] and is a characteristic of J-aggregate formation [56].

Annealing in the air at 200 °C for 3 h had no significant effect on thin films. The observed diffraction peaks are slightly shifted to the right (interplanar values become smaller), which is caused by the release of mechanical stress in thin films. Assuming that the instrumental peak broadening is 0.05° (measured from an SRM−660a LaB_6 powder sample), the size of the coherent scattering region for each film was estimated using the

Scherrer equation and equal to 16.9 nm for $ZnPcF_8$, 85 nm for $CoPcF_8$, and 27.2 nm for $VOPcF_8$. After annealing, these values became 16.6 nm, 73 nm, and 26.8 nm, respectively. The angles between phthalocyanine molecules (least squares plane through all atoms except hydrogen, oxygen, and vanadium) and the substrate surface, determined on the basis of the crystal structure data, were 70.36° for $ZnPcF_8$, 75.45° for $CoPcF_8$, and 86.82° for $VOPcF_8$. The UV-vis spectra of $CoPcF_8$ and $ZnPcF_8$ films after heating also did not undergo noticeable changes. In the UV-vis spectrum of $VOPcF_8$, the Q-band only became broader.

2.5. Study of The Conductivity of $MPcF_8$ Films

To investigate the effect of the central metal ion on conductivity, the I(V) dependencies of as-deposited $MPcF_8$ (M=Zn(II), Co(II), VO) films were measured using a Keithley 236 electrometer (Figure 10a,b). For this purpose, the films were deposited on glass substrates with interdigitated Pt electrodes. A $CoPcF_8$ film demonstrates ohmic conductivity in the investigated range from 0 to 10 V. The I(V) dependencies of $ZnPcF_8$ and $VOPcF_8$ are linear below 3 V and 2.5 V, respectively, while the shape of curves changes above these values with the slopes of a log$I$ versus log$V$ at about 1.3 for $ZnPcF_8$ and 1.7 for $VOPcF_8$. These values are below $n = 2$ in the dependence of $I \propto V^n$, which is typical for the space-charge-limited conduction (SCL) mechanism [57]. In the case of the investigated $MPcF_8$ (M=Zn(II), Co(II), VO) films, the ohmic conduction mechanism dominated the SCL conduction. The lateral d.c. conductivity ($\sigma_{//}$) estimated in the linear range was close for the films of $ZnPcF_8$ ($1.9 \cdot 10^{-9}$ $\Omega^{-1}m^{-1}$) and $VOPcF_8$ ($1.3 \cdot 10^{-9}$ $\Omega^{-1}m^{-1}$). The $\sigma_{//}$ of $CoPcF_8$ was noticeably higher and equal to $6.2 \cdot 10^{-4}$ $\Omega^{-1}m^{-1}$. The conductivity of $MPcF_8$ films was also compared with that of their tetrafluorinated analogues (Figure 10a,b).

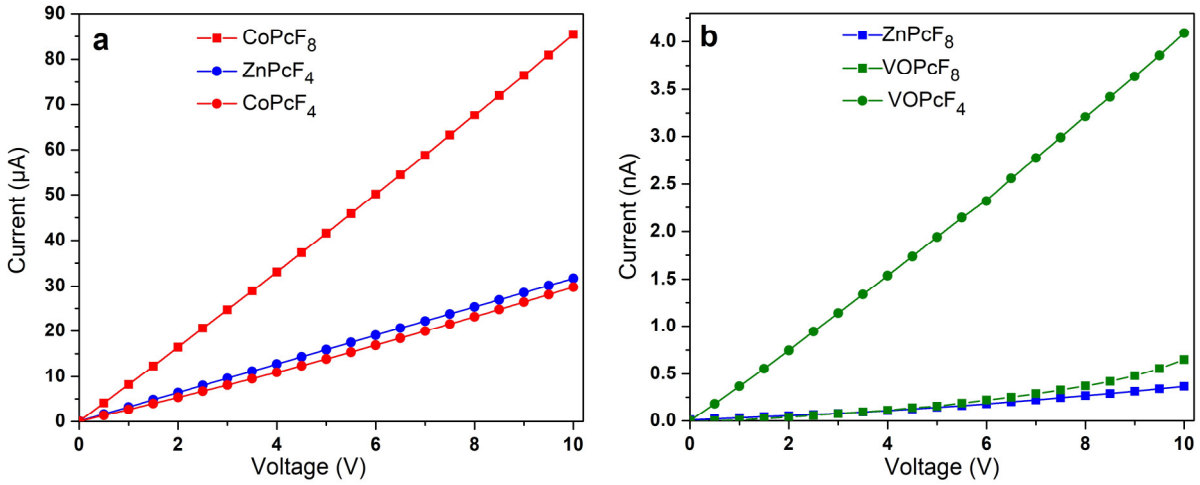

Figure 10. *I(V)* dependencies of $CoPcF_8$ (**a**) and $ZnPcF_8$, $VOPcF_8$ (**b**) thin films in comparison with their tetrafluoro-substituted analogues $CoPcF_4$-p, $ZnPcF_4$-p (**a**) and $VOPcF_4$-p (**b**).

The conductivity and charge-carrier mobility of polycrystalline MPc films are determined both by the packing of phthalocyanine molecules in the crystallite and by the morphology of the film. Jiang with co-authors [37,58] studied the dependence of the charge-carrier mobility in MPc single crystals on the distances between neighboring molecules along the shortest axis with the closest parallel π-stackings. It was shown that as the intermolecular distances along their shortest packing axis in unsubstituted H_2Pc and MPcs decreased, the hole mobility gradually increased. This approach is reasonable in the case of isostructural phthalocyanines. $CoPcF_8$ and $ZnPcF_8$ investigated in this work have different structures; the distances between neighboring molecules in stacks are very close but the packing motifs are different, which leads to the different π–π interactions

between neighboring molecules in the stack. It was shown above using HS analysis that in the case of $ZnPcF_8$ only pyrrole moieties participate in one π–π interaction, while in the case of $CoPcF_8$ the whole molecule is involved in π–π interaction with neighboring molecules in the stack (Figure 5). Such a better overlap of π-orbitals may contribute to an increase in the conductivity of $CoPcF_8$ films. Moreover, according to the XRD analysis, there are no disordered atoms in the structure of $CoPcF_8$, which leads to better crystallinity of the films because the fewer defects and microstresses in the crystal lattice, the better the crystallinity of the films. This fact in turn may lead to the better conductivity of $CoPcF_8$ films. The same character of interactions as in $CoPcF_8$ was also observed in $ZnPcF_4$-p and $CoPcF_4$-p [13]. The $\sigma_{//}$ values of the films of these phthalocyanines were comparable with the conductivity of $CoPcF_8$ films and equal to $2.1 \cdot 10^{-4}$ and $2.6 \cdot 10^{-4}$ $\Omega^{-1}m^{-1}$ for $ZnPcF_4$-p and $CoPcF_4$-p, respectively.

Vanadyl phthalocyanine molecules have a different packaging style due to their non-planar structure. HS of $VOPcF_8$ (Figure 5) showed that four benzene rings of each molecule form two pairs of π–π bonds with two adjacent molecules, making molecular chains. Comparison of HS shows that $VOPcF_4$ ($2.9 \cdot 10^{-8}$ $\Omega^{-1}m^{-1}$) has more π–π contacts than $VOPcF_8$, including contacts between benzene fragments and between the benzene ring and macrocycle of the adjacent molecule [13].

3. Materials and Methods

$ZnPcF_8$, $CoPcF_8$, and $VOPcF_8$ were synthesized by template synthesis [59] by fusing a mixture (4:1) of difluorophthalonitrile (abcr, Karlsruhe, Germany, CAS 134450–56–9) with salts of the corresponding metals, viz., zinc acetate dihydrate (Sigma-Aldrich, Saint Louis, MO, USA, CAS 5970–45–6), $CoCl_2$ 391 (Sigma-Aldrich, Saint Louis, MO, USA, CAS 7746–79–9), or VCl_3 (Sigma-Aldrich, Saint Louis, MO, USA, CAS 7718–98–1), respectively. Difluorophthalonitrile and the corresponding amount (4:1 molar ratio) of a metal salt were ground in a mortar and placed in an ampoule. The mixture was heated at 190–210 °C for several hours, then the resulting dark blue or dark green solid product was crushed and placed in a new clean ampoule for subsequent purification by sublimation. The resulting powders were purified twice by sublimation in a vacuum (10^{-5} Torr); the yield after sublimation was around 50%.

As a result of sublimation, single crystals of $ZnPcF_8$, $CoPcF_8$, and $VOPcF_8$ were obtained.

$ZnPcF_8$: $C_{32}H_8F_8N_8Zn$. Anal. Calc: C, 53.2; H, 1.1; N, 15.5; F, 21.1%. Found: C, 53.4; H, 1.3; N, 15.5; F, 21.0%. IR spectrum (KBr; ω, cm−1): 1618; 1603; 1489; 1465; 1339; 1281; 1204; 1178; 1140; 1086; 1026; 889; 870; 814; 746; 615; 559; 503; 441.

$CoPcF_8$: $C_{32}H_8F_8N_8Co$. Anal. Calc: C, 53.7; H, 1.1; N, 15.7; F, 21.2%. Found: C, 53.8; H, 1.1; N, 15.9; F, 21.4%. IR spectrum (KBr; ω, cm^{-1}): 1620; 1601; 1506; 1472; 1423; 1337; 1286; 1211; 1184; 1142; 1074; 1034; 895; 878; 818; 752; 688; 615; 567; 503; 447.

$VOPcF_8$: $C_{32}H_8F_8N_8VO$. Anal. Calc: C, 53.1; H, 1.1; N, 15.5; F, 21.0%. Found: C, 53.3; H, 1.2; N, 15.6; F, 21.1%. IR spectrum (KBr; ω, cm^{-1}): 1620; 1609; 1528; 1499; 1475; 1433; 1347; 1287; 1208; 1182; 1146; 1092; 1045; 930; 885; 870; 822; 750; 669; 617; 567; 511; 442.

Thin films of $ZnPcF_8$, $CoPcF_8$, and $VOPcF_8$ were deposited by an OMBD technique at a residual pressure of 10^{-5} Torr and evaporation temperature of 450–460 °C. Glass slides were used as substrates. The films' thicknesses were determined by the method of spectral ellipsometry using a spectroscopic ellipsometer ELLIPS 1771 SA (ISP, Novosibirsk, Russia) [60] as described in our previous work [61]; thicknesses were determined to be 85, 80, and 87 nm for $ZnPcF_8$, $CoPcF_8$, and $VOPcF_8$ films, respectively.

IR and Raman spectra were recorded with a Vertex 80 FTIR spectrometer (Ettlingen, Germany) and a LabRAM Horiba single spectrometer (Montpellier, France) (488 nm line of an Ar+ laser), respectively.

Crystal structure data were obtained using a single-crystal diffractometer Bruker X8 (sealed Mo-anode tube with a graphite monochromator, 4-circle goniometer, APEX II CCD detector) and Venture single-crystal diffractometer Bruker D8 (Billerica, MA, USA)

(Incoatec IμS 3.0 microfocus X-ray source with Mo-anode, 3-circle goniometer, PHOTON III C14 CPAD detector). Both diffractometers were equipped with Oxford Cryosystems Cryostream 800 (Oxford, United Kingdom) plus open-flow nitrogen coolers, which were used to maintain the sample temperature at 150(±2) K. The data acquisition strategy consisted of several ω-scans with 0.5° wide frames. The raw data frame collection, data reduction, absorption correction, and global unit cell refinement were performed in the APEX3 V2018.7–2 software package (SAINT 8.38A, SADABS−2016/2) (Madison, Wisconsin, USA) [62]. The resulting hkl datasets were processed in Olex2 v.1.5 10 (Durham, United Kingdom) [63] using SHELXT 2018/2 [64] and SHELXL 2018/3 [65] (Göttingen, Germany) for the structure solution and refinement. $ZnPcF_8$, $CoPcF_8$, and $VOPcF_8$ structural data were deposited to The Cambridge Crystallographic Data Centre (CCDC) with the numbers 2177575, 2177576, and 2177577 and can be obtained from https://www.ccdc.cam.ac.uk/structures/ (accessed on 5 July 2022).

Powder and thin film diffraction patterns were obtained in the 2θ range of 3–40° using a Bruker D8 (Billerica, MA, USA) advance powder diffractometer (vertical θ-θ goniometer in the Bragg-Brentano geometry, Cu-anode sealed tube without a β-filter 40mA @ 40 kV, LYNXEYE XE-T compound silicon strip detector, motorized divergence slit), with a step of 0.01023°, an acquisition time of 2 s/step, and a fixed sample illumination area.

Electronic absorption spectra of MPcF8 solutions and films were recorded using a UV–Vis−3101PC ''Shimadzu'' (Kyoto, Japan) scanning spectrophotometer.

I(V) dependencies of $MPcF_8$ films were measured using a Keithley 236 electrometer. The films were deposited onto glass slides with Pt IDE (Metrohm, DropSens, Spain, the dimension of the gaps was 10 μm; the number of digits was 125 × 2 with a digit length equal to 6760 μm).

4. Conclusions

In this work, octafluoro-substituted phthalocyanines of zinc, vanadyl, and cobalt ($MPcF_8$, M=Zn(II), Co(II), VO) were synthesized and studied. The structures of $CoPcF_8$ and $VOPcF_8$ single crystals were determined for the first time. $CoPcF_8$ crystallizes in a triclinic system with Z=1 and a space group P−1 and is isostructural to α-CoPc and previously reported $CoPcF_4$-p and $CuPcF_8$. $VOPcF_8$ also crystallizes in a P−1 space group but with Z=2. Judging from the unit cell parameters, this minor phase of $ZnPcF_8$ is isostructural to $CoPcF_8$ and $CuPcF_8$.

It was shown that the presence of eight peripheral F-substituents has a different effect on molecular packing and intermolecular contacts in different $MPcF_8$. In the case of $CoPcF_8$, no significant changes were observed compared to α-CoPc and $CoPcF_4$-p. $ZnPcF_8$ molecules are packed in a staggered manner, forming two-dimensional molecular layers, usually observed in non-planar phthalocyanines. The number of π–π interactions between $ZnPcF_8$ molecules decreased compared to $ZnPcF_4$-p. $VOPcF_8$ molecules are packed in molecular chains that are connected to each other along the *b* axis. Compared to $VOPcF_4$-p, close F…F and F…H contacts between $VOPcF_8$ molecules are much weaker.

All three studied $MPcF_8$ formed highly oriented single-phase thin films when deposited onto glass substrates using a PVD method. Their crystal phases correspond to the crystal structure of single crystals. The angles between the macrocycle plane and the substrate surface were 70.36° for $ZnPcF_8$, 77.17° for $CoPcF_8$, and 86.82° for $VOPcF_8$.

Author Contributions: Conceptualization, D.K. and T.B.; methodology, A.S. and T.B.; software, A.S.; validation, A.S. and D.K.; formal analysis, A.S. and D.B.; investigation, A.S., D.B. and D.K.; writing—original draft preparation, A.S., D.K. and T.B.; writing—review and editing, D.K. and T.B.; visualization, A.S.; supervision, T.B.; project administration, D.K.; funding acquisition, D.K. All authors have read and agreed to the published version of the manuscript.

Funding: The study of vanadyl phthalocyanine crystals, powders and films was funded by the Russian Science Foundation, grant number 22−73−00145.

Institutional Review Board Statement: Not applicable.

Informed Consent Statement: Not applicable.

Data Availability Statement: The data presented in this study are available on request from the corresponding author. $ZnPcF_8$, $CoPcF_8$, and $VOPcF_8$ structural data can be obtained from https://www.ccdc.cam.ac.uk/structures/ (accessed on 5 July 2022) (numbers 2177575, 2177576, and 2177577).

Acknowledgments: The authors acknowledge the Ministry of Science and Higher Education of the Russian Federation (N 121031700314−5 and N 121031700313−8) for access to the center of collective use to study films of cobalt and zinc phthalocyanines.

Conflicts of Interest: The authors declare no conflict of interest.

References

1. Gümrükçü Köse, G.; Karaoğlan, G.K.; Erdağ Maden, Y.; Koca, A. Novel silicon phthalocyanine photosensitizers containing carboxylic acid based axial anchoring groups: Electrochemistry, spectroelectrochemistry, and dye sensitized solar cell performance. *Dyes Pigments* **2022**, *207*, 110686, doi:10.1016/J.DYEPIG.2022.110686.
2. Şenoğlu, S.; Özer, M.; Dumludağ, F.; Acar, N.; Salih, B.; Bekaroğlu, Ö. Synthesis, characterization, DFT study, conductivity and effects of humidity on CO2 sensing properties of the novel tetrakis-[2-(dibenzylamino)ethoxyl] substituted metallophthalocyanines. *Sensors Actuators, B Chem.* **2020**, *310*, 127860, doi:10.1016/j.snb.2020.127860.
3. Bunin, D.A.; Martynov, A.G.; Safonova, E.A.; Tsivadze, A.Y.; Gorbunova, Y.G. Robust route toward cationic phthalocyanines through reductive amination. *Dyes Pigments* **2022**, *207*, 110768, doi:10.1016/J.DYEPIG.2022.110768.
4. Yahya, M.; Nural, Y.; Seferoğlu, Z. Recent advances in the nonlinear optical (NLO) properties of phthalocyanines: A review. *Dye. Pigment.* **2022**, *198*, 109960, doi:10.1016/J.DYEPIG.2021.109960.
5. Lukyanets, E.A. Phthalocyanines as Photosensitizers in the Photodynamic Therapy of Cancer. *J. Porphyr. Phthalocyanines* **1999**, *3*, 424–432, doi:10.1002/(sici)1099-1409(199908/10)3:6/7<424::aid-jpp151>3.0.co;2-k.
6. de Oliveira, M.S.; Farias, E.A. de O.; de Sousa, A.M.S.; Dionísio, N.A.; Teixeira, P.R.S.; Teixeira, A.S. do N.M.; da Silva, D.A.; Eiras, C. Composite films based on copper nanoparticles and nickel phthalocyanine as electrochemical sensors for serotonin detection. *Surfaces and Interfaces* **2021**, *25*, 101245, doi:10.1016/J.SURFIN.2021.101245.
7. Zheng, B. De; Ye, J.; Zhang, X.Q.; Zhang, N.; Xiao, M.T. Recent advances in supramolecular activatable phthalocyanine-based photosensitizers for anti-cancer therapy. *Coord. Chem. Rev.* **2021**, *447*, 214155, doi:10.1016/J.CCR.2021.214155.
8. Szymczak, J.; Rebis, T.; Kotkowiak, M.; Wicher, B.; Sobotta, L.; Tykarska, E.; Mielcarek, J.; Kryjewski, M. Regioisomers of magnesium(II) phthalocyanine bearing menthol substituents–Synthesis, spectral, electrochemical and computational studies. *Dyes Pigments* **2021**, *191*, 109357, doi:10.1016/J.DYEPIG.2021.109357.
9. Ivanova, V.; Klyamer, D.; Krasnov, P.; Kaya, E.N.; Kulu, I.; Tuncel Kostakoğlu, S.; Durmuş, M.; Basova, T. Hybrid materials based on pyrene-substituted metallo phthalocyanines as sensing layers for ammonia detection: Effect of the number of pyrene substituents. *Sensors Actuators B Chem.* **2023**, *375*, 132843, doi:10.1016/J.SNB.2022.132843.
10. Robin Nxele, S.; Nkhahle, R.; Nyokong, T. The composites of asymmetric Co phthalocyanines-graphitic carbon nitride quantum dots-aptamer as specific electrochemical sensors for the detection of prostate specific antigen: Effects of ring substituents. *J. Electroanal. Chem.* **2021**, *900*, 115730, doi:10.1016/J.JELECHEM.2021.115730.
11. Chen, Y.; Yao, Q.; Qu, S.; Shi, W.; Li, H.; Chen, L. Enhanced thermoelectric performance of phthalocyanine complexes/single-walled carbon nanotube hybrids by tuning the types of metal coordination ions. *Compos. Commun.* **2021**, *27*, 100891, doi:10.1016/J.COCO.2021.100891.
12. Zeinidenov, A.K.; Aimukhanov, A.K.; Kambar, D.S.; Ilyassov, B.R.; Zavgorodniy, A. V. Effects of phthalocyanine nanostructure on photovoltaic performance of its polymer composite thin films. *Mater. Chem. Phys.* **2021**, *267*, 124680, doi:10.1016/J.MATCHEMPHYS.2021.124680.
13. Klyamer, D.D.; Sukhikh, A.S.; Trubin, S. V.; Gromilov, S.A.; Morozova, N.B.; Basova, T. V.; Hassan, A.K. Tetrafluorosubstituted Metal Phthalocyanines: Interplay between Saturated Vapor Pressure and Crystal Structure. *Cryst. Growth Des.* **2020**, *20*, 1016–1024, doi:10.1021/acs.cgd.9b01350.
14. Basova, T.; Semyannikov, P.; Plyashkevich, V.; Hassan, A.; Igumenov, I. Volatile phthalocyanines: Vapor pressure and thermodynamics. *Crit. Rev. Solid State Mater. Sci.* **2009**, *34*, 180–189, doi:10.1080/10408430903245377.
15. Matumoto, A.; Hoshino, N.; Akutagawa, T.; Matsuda, M. N-type semiconducting behavior of copper octafluorophthalocyanine in an organic field-effect transistor. *Appl. Sci.* **2017**, *7*, doi:10.3390/app7111111.
16. Bao, Z.; Lovinger, A.J.; Brown, J. New air-stable n-channel organs thin film transistors. *J. Am. Chem. Soc.* **1998**, *120*, 207–208, doi:10.1021/ja9727629.
17. Ling, M.-M.; Bao, Z.; Erk, P. Air-stable n-channel copper hexachlorophthalocyanine for field-effect transistors. *Appl. Phys. Lett.* **2006**, *89*, 163516, doi:10.1063/1.2362976.
18. 18. Lessard, B.H. The Rise of Silicon Phthalocyanine: From Organic Photovoltaics to Organic Thin Film Transistors. *ACS Appl. Mater. & Interfaces* **2021**, *13*, 31321–31330, doi:10.1021/acsami.1c06060.

19. Gai, S.; Wang, B.; Wang, X.; Zhang, R.; Miao, S.; Wu, Y. Ultrafast NH_3 gas sensor based on phthalocyanine-optimized non-covalent hybrid of carbon nanotubes with pyrrole. *Sensors Actuators B Chem.* **2022**, *357*, 131352, doi:10.1016/J.SNB.2021.131352.
20. Carvalho da Silva, V.N.; Farias, E.A. de O.; Araújo, A.R.; Xavier Magalhães, F.E.; Neves Fernandes, J.R.; Teles Souza, J.M.; Eiras, C.; Alves da Silva, D.; Hugo do Vale Bastos, V.; Teixeira, S.S. Rapid and selective detection of dopamine in human serum using an electrochemical sensor based on zinc oxide nanoparticles, nickel phthalocyanines, and carbon nanotubes. *Biosens. Bioelectron.* **2022**, *210*, 114211, doi:10.1016/J.BIOS.2022.114211.
21. Bouvet, M.; Guillaud, G.; Leroy, A.; Maillard, A.; Spirkovitch, S.; Tournilhac, F.-G. Phthalocyanine-based field-effect transistor as ozone sensor. *Sensors Actuators B Chem.* **2001**, *73*, 63–70, doi:10.1016/S0925-4005(00)00682-1.
22. Sukhikh, A.S.; Klyamer, D.D.; Parkhomenko, R.G.; Krasnov, P.O.; Gromilov, S.A.; Hassan, A.K.; Basova, T. V. Effect of fluorosubstitution on the structure of single crystals, thin films and spectral properties of palladium phthalocyanines. *Dye. Pigment.* **2018**, *149*, 348–355, doi:10.1016/j.dyepig.2017.10.024.
23. Sukhikh, A.; Bonegardt, D.; Klyamer, D.; Basova, T. Effect of non-peripheral fluorosubstitution on the structure of metal phthalocyanines and their films. *Dyes Pigments* **2021**, *192*, 109442, doi:10.1016/j.dyepig.2021.109442.
24. Klyamer, D.; Sukhikh, A.; Nikolaeva, N.; Morozova, N.; Basova, T. Vanadyl phthalocyanine films and their hybrid structures with Pd nanoparticles: Structure and sensing properties. *Sensors* **2020**, *20*, 1893, doi:10.3390/s20071893.
25. Yoon, S.M.; Song, H.J.; Hwang, I.C.; Kim, K.S.; Choi, H.C. Single crystal structure of copper hexadecafluorophthalocyanine (F_{16}CuPc) ribbon. *Chem. Commun.* **2010**, *46*, 231–233, doi:10.1039/b914457a.
26. Jiang, H.; Ye, J.; Hu, P.; Wei, F.; Du, K.; Wang, N.; Ba, T.; Feng, S.; Kloc, C. Fluorination of metal phthalocyanines: Single-crystal growth, efficient N-channel organic field-effect transistors, and structure-property relationships. *Sci. Rep.* **2014**, *4*, 1–6, doi:10.1038/srep07573.
27. Ma, F.; Wang, S.; Li, X. Synthesis, spectral characterization of $CuPcF_{16}$ and its application in organic thin film transistors using p-6p as inducing layer. *J. Phys. Chem. Solids* **2012**, *73*, 589–592, doi:10.1016/J.JPCS.2011.12.016.
28. Klyamer, D.; Sukhikh, A.; Gromilov, S.; Krasnov, P.; Basova, T. Fluorinated metal phthalocyanines: Interplay between fluorination degree, films orientation, and ammonia sensing properties. *Sensors* **2018**, *18*, 2141, doi:10.3390/s18072141.
29. Dong, N.; Wu, X.-M.; Dang, H.-Q.; Liu, D.-Y.; Zhang, Q.; Wei, J.; Yin, S.-G. Improved Performance of Phthalocyanine Derivative Field-Effect Transistors by Inserting a Para-Quarterphenyl as the Inducing Layer. *Chinese Phys. Lett.* **2014**, *31*, 058501, doi:10.1088/0256-307X/31/5/058501.
30. Bouvet, M.; Gaudillat, P.; Kumar, A.; Sauerwald, T.; Schüler, M.; Schütze, A.; Suisse, J.M. Revisiting the electronic properties of Molecular Semiconductor–Doped Insulator (MSDI) heterojunctions through impedance and chemosensing studies. *Org. Electron.* **2015**, *26*, 345–354, doi:10.1016/j.orgel.2015.07.052.
31. Kumar, A.; Meunier-Prest, R.; Bouvet, M. Organic heterojunction devices based on phthalocyanines: A new approach to gas chemosensing. *Sensors (Switzerland)* **2020**, *20*, 1–25, doi:10.3390/s20174700.
32. Kuprikova, N.M.; Klyamer, D.D.; Sukhikh, A.S.; Krasnov, P.O.; Mrsic, I.; Basova, T. V. Fluorosubstituted lead phthalocyanines: Crystal structure, spectral and sensing properties. *Dyes Pigments* **2020**, *173*, 107939, doi:10.1016/j.dyepig.2019.107939.
33. Bonegardt, D.; Klyamer, D.; Sukhikh, A.; Krasnov, P.; Popovetskiy, P.; Basova, T. Fluorination vs . Chlorination : Effect on the Sensor Response of Tetrasubstituted Zinc Phthalocyanine Films to Ammonia. **2021**, *9*, 137, doi:10.3390/chemosensors9060137.
34. Shao, X.; Wang, S.; Li, X.; Su, Z.; Chen, Y.; Xiao, Y. Single component p-, ambipolar and n-type OTFTs based on fluorinated copper phthalocyanines. *Dyes Pigments* **2016**, *132*, 378–386, doi:10.1016/J.DYEPIG.2016.05.020.
35. Brinkmann, H.; Kelting, C.; Makarov, S.; Tsaryova, O.; Schnurpfeil, G.; Wöhrle, D.; Schlettwein, D. Fluorinated phthalocyanines as molecular semiconductor thin films. *Phys. Status Solidi Appl. Mater. Sci.* **2008**, *205*, 409–420, doi:10.1002/pssa.200723391.
36. Peisert, H.; Knupfer, M.; Fink, J. Electronic structure of partially fluorinated copper phthalocyanine ($CuPcF_4$) and its interface to Au(1 0 0). *Surf. Sci.* **2002**, *515*, 491–498, doi:10.1016/S0039-6028(02)01967-2.
37. Jiang, H.; Hu, P.; Ye, J.; Li, Y.; Li, H.; Zhang, X.; Li, R.; Dong, H.; Hu, W.; Kloc, C. Molecular Crystal Engineering: Tuning Organic Semiconductor from p-type to n-type by Adjusting Their Substitutional Symmetry. *Adv. Mater.* **2017**, *29*, 1605053, doi:10.1002/adma.201605053.
38. Konarev, D.V.; Troyanov, S.I.; Kuzmin, A.V.; Nakano, Y.; Ishikawa, M.; Faraonov, M.A.; Khasanov, S.S.; Litvinov, A.L.; Otsuka, A.; Yamochi, H.; et al. The Salts of Copper Octafluoro- and Hexadecafluorophthalocyanines Containing $[Cu^{II}(F_8Pc)^{4-}]^{2-}$ Dianions and $[CuF_{16}Pc]^-$ Monoanions. *Inorg. Chem.* **2017**, *56*, 1804–1813, doi:10.1021/acs.inorgchem.6b01932.
39. Oison, V.; Koudia, M.; Abel, M.; Porte, L. Influence of stress on hydrogen-bond formation in a halogenated phthalocyanine network. *Phys. Rev. B–Condens. Matter Mater. Phys.* **2007**, *75*, 1–6, doi:10.1103/PhysRevB.75.035428.
40. Giovanelli, L.; Bocquet, F.C.; Amsalem, P.; Lee, H.-L.; Abel, M.; Clair, S.; Koudia, M.; Faury, T.; Petaccia, L.; Topwal, D.; et al. Interpretation of valence band photoemission spectra at organic-metal interfaces. *Phys. Rev. B* **2013**, *87*, 35413, doi:10.1103/PhysRevB.87.035413.
41. Ballirano, P.; Caminiti, R.; Ercolani, C.; Maras, A.; Orrù, M.A. X-ray powder diffraction structure reinvestigation of the α and β forms of cobalt phthalocyanine and kinetics of the $\alpha \rightarrow \beta$ phase transition. *J. Am. Chem. Soc.* **1998**, *120*, 12798–12807, doi:10.1021/ja973815p.
42. Ziolo, R.F.; Griffiths, C.H.; Troup, J.M. Crystal structure of vanadyl phthalocyanine, phase II. *J. Chem. Soc. Dalt. Trans.* **1980**, 2300–2302, doi:10.1039/DT9800002300.

43. Spackman, P.R.; Turner, M.J.; McKinnon, J.J.; Wolff, S.K.; Grimwood, D.J.; Jayatilaka, D.; Spackman, M.A. CrystalExplorer: A program for Hirshfeld surface analysis, visualization and quantitative analysis of molecular crystals. *J. Appl. Crystallogr.* **2021**, *54*, 1006–1011, doi:10.1107/S1600576721002910.
44. Klyamer, D.D.; Sukhikh, A.S.; Gromilov, S.A.; Kruchinin, V.N.; Spesivtsev, E. V.; Hassan, A.K.; Basova, T. V. Influence of fluorosubstitution on the structure of zinc phthalocyanine thin films. *Macroheterocycles* **2018**, *11*, 304–311, doi:10.6060/mhc180794b.
45. Klyamer, D.D.; Basova, T. V.; Krasnov, P.O.; Sukhikh, A.S. Effect of fluorosubstitution and central metals on the molecular structure and vibrational spectra of metal phthalocyanines. *J. Mol. Struct.* **2019**, *1189*, 73–80, doi:10.1016/j.molstruc.2019.04.032.
46. Tackley, D.R.; Dent, G.; W. Smith W.E. IR and Raman assignments for zinc phthalocyanine from DFT calculations. *Phys. Chem. Chem. Phys*. **2000**, *2*, 3949-3955, doi: 10.1039/b005091l.
47. Tackley, D.R.; Dent, G.; Smith, W.E. Phthalocyanines: Structure and vibrations. *Phys. Chem. Chem. Phys.* **2001**, *3*, 1419–1426, doi:10.1039/b007763l. Daniel R. Tackley,a Geoꞇrey Dentb and W. Ewen Smith
48. Basova, T. V.; Kiselev, V.G.; Schuster, B.E.; Peisert, H.; Chassé, T. Experimental and theoretical investigation of vibrational spectra of copper phthalocyanine: Polarized single-crystal Raman spectra, isotope effect and DFT calculations. *J. Raman Spectrosc.* **2009**, *40*, 2080–2087, doi:10.1002/jrs.2375.
49. Cranston, R.R.; Lessard, B.H. Metal phthalocyanines: thin-film formation, microstructure, and physical properties. *RSC Adv.* **2021**, *11*, 21716–21737, doi:10.1039/d1ra03853b.
50. Fronk, M.; Bräuer, B.; Zahn, D.R.T.; Salvan, G. Temperature dependence of the optical anisotropy of vanadyl phthalocyanine films. *Thin Solid Films* **2008**, *516*, 7916–7920, doi:10.1016/J.TSF.2008.04.094.
51. Kerp, H.R.; Westerduin, K.T.; Van Veen, A.T.; Van Faassen, E.E. Quantification and effects of molecular oxygen and water in zinc phthalocyanine layers. *J. Mater. Res.* **2001**, *16*, 503–511, doi:10.1557/JMR.2001.0073.
52. van Faassen, E.E.; Schlettwein, D. Energy Migratoin and Light-Induced Charge Transfer at Phthalocyanine Surfaces. In *Handbook of Photochemistry and Photobiology, Vol. 3: Supramolecular Photochemistry*; Nalwa, H.S., Ed.; American Scientific: California, 2003; pp. 355–409.
53. Klyamer, D.D.; Sukhikh, A.S.; Krasnov, P.O.; Gromilov, S.A.; Morozova, N.B.; Basova, T. V. Thin films of tetrafluorosubstituted cobalt phthalocyanine: Structure and sensor properties. *Appl. Surf. Sci.* **2016**, *372*, 79–86, doi:10.1016/j.apsusc.2016.03.066.
54. Ji, X.; Zou, T.; Gong, H.; Wu, Q.; Qiao, Z.; Wu, W.; Wang, H. Cobalt phthalocyanine nanowires: Growth, crystal structure, and optical properties. *Cryst. Res. Technol.* **2016**, *51*, 154–159, doi:10.1002/crat.201500244.
55. Yamashita, A.; Maruno, T.; Hayashi, T. Absorption spectra of organic-molecular-beam-deposited vanadyl- and titanylphthalocyanine. *J. Phys. Chem.* **2002**, *97*, 4567–4569, doi:10.1021/j100120a001.
56. Zhang, X.F.; Xi, Q.; Zhao, J. Fluorescent and triplet state photoactive J-type phthalocyanine nano assemblies: Controlled formation and photosensitizing properties. *J. Mater. Chem.* **2010**, *20*, 6726–6733, doi:10.1039/c0jm00695e.
57. Chiu, F. A Review on Conduction Mechanisms in Dielectric Films. *Adv. Mater. Sci. Eng.* **2014**, *1*, 1–18, doi:10.1155/2014/578168.
58. Jiang, H.; Hu, P.; Ye, J.; Ganguly, R.; Li, Y.; Long, Y.; Fichou, D.; Hu, W.; Kloc, C. Hole Mobility Modulation in Single-Crystal Metal Phthalocyanines by Changing the Metal–π/π–π Interactions. *Angew. Chemie–Int. Ed.* **2018**, *57*, 10112–10117, doi:10.1002/anie.201803363.
59. Stuzhin, P.A. Fluorinated phthalocyanine and their analogues. In *Fluorine in Heterocyclic Chemistry: Volume 1: 5-Membered Heterocycles and Macrocycles*; Nenajdenko, V., Ed.; Springer International Publishing, 2014; Vol. 1, pp. 621–681 ISBN 9783319043463.
60. Spesivtsev, E. V.; Rykhlitskii, S. V.; Shvets, V.A. Development of methods and instruments for optical ellipsometry at the Institute of Semiconductor Physics of the Siberian Branch of the Russian Academy of Sciences. *Optoelectron. Instrum. Data Process.* **2011**, *47*, 419–425, doi:10.3103/s8756699011050219.
61. Kruchinin, V.N.; Klyamer, D.D.; Spesivtsev, E. V.; Rykhlitskii, S. V.; Basova, T. V. Optical Properties of Thin Films of Zinc Phthalocyanines Determined by Spectroscopic Ellipsometry. *Opt. Spectrosc.* **2018**, *125*, 1019–1024, doi:10.1134/S0030400X18120093.
62. Bruker AXS Inc Bruker Advanced X-ray Solutions, Madison, Wisconsin, USA 2004.
63. Dolomanov, O. V.; Bourhis, L.J.; Gildea, R.J.; Howard, J.A.K.; Puschmann, H. OLEX2: A complete structure solution, refinement and analysis program. *J. Appl. Crystallogr.* **2009**, *42*, 339–341, doi:10.1107/S0021889808042726.
64. Sheldrick, G.M. SHELXT–Integrated space-group and crystal-structure determination. *Acta Crystallogr. Sect. A Found. Crystallogr.* **2015**, *71*, 3–8, doi:10.1107/S2053273314026370.
65. Sheldrick, G.M. Crystal structure refinement with SHELXL. *Acta Crystallogr. Sect. C Struct. Chem.* **2015**, *71*, 3–8, doi:10.1107/S2053229614024218.